Thermodynamic Redox Behavior of the Heme Centers in A-Type Heme-Copper Oxygen Reductases: Comparison between the Two Subfamilies

Andreia F. Veríssimo, Filipa L. Sousa, António M. Baptista, Miguel Teixeira, and Manuela M. Pereira
Instituto de Tecnologia Química e Biológica, Universidade Nova de Lisboa, Oeiras, Portugal

ABSTRACT The study of the thermodynamic redox behavior of the hemes from two members of the A family of heme-copper oxygen reductases, *Paracoccus denitrificans* aa_3 (A1 subfamily) and *Rhodothermus marinus* caa_3 (A2 subfamily) enzymes, is presented. At different pH values, midpoint reduction potentials and interaction potentials were obtained in the framework of a pairwise model for two interacting redox centers. In both enzymes, the hemes have different reduction potentials. For the A1-type enzyme, it was shown that heme *a* has a pH-dependent midpoint reduction potential, whereas that of heme a_3 is pH independent. For the A2-type enzyme the opposite was observed. The midpoint reduction potential of heme *c* from subunit II of the caa_3 enzyme was determined by fitting the data with a single-electron Nernst curve, and it was shown to be pH dependent. The results presented here for these A-type enzymes are compared with those previously obtained for representative members of the B and C families.

INTRODUCTION

Oxygen reductases are the last enzymatic complexes of aerobic respiratory chains that catalyze the reduction of dioxygen to water. Most respiratory oxygen reductases are members of the heme-copper superfamily (1–5) and couple dioxygen reduction to the translocation of protons across the membrane. The electrons for the catalytic reaction are provided by the oxidation of periplasmatic proteins or membrane diffusing quinols. The charge separation promoted by the catalytic reaction and proton pumping leads to the establishment of a transmembrane difference of electrochemical potential that may be used by ATP synthase for the production of ATP from ADP and inorganic phosphate, as well as for other membrane-potential-dependent processes.

Taking into consideration the overall amino acid sequences of the core subunits, the amino acid residues involved in proton transfer (4), and the properties of the catalytic center (6), the heme-copper oxygen reductases superfamily was organized into three different families, named A, B, and C (4). Only subunit I is common to all. It contains the catalytic binuclear dioxygen reducing site, which is composed of a high-spin heme and a copper ion (Cu_B) and its immediate electron donor, a low-spin heme. All oxygen reductases have at least another subunit, which for the members of the A and B families is designated as subunit II. In oxygen reductases that oxidize periplasmatic metalloproteins, this subunit has a binuclear copper center (Cu_A) and in some cases a C-terminal extension harboring at least one heme *c*. In quinol oxidases, no prosthetic group is found in subunit II. All C-type oxygen reductases are cbb_3-type enzymes, which besides the catalytic subunit I have a monohemic and a dihemic cytochrome *c* subunit (4).

The mitochondrial enzyme is included in the A family, which is further subdivided into two subfamilies: A1 and A2. The members of the A1 subfamily (e.g., the aa_3 oxygen reductase from *Paracoccus denitrificans*, bo_3 from *Escherichia coli*, and caa_3 from *Bacillus subtilis*) have all the amino acid residues constituting the D- and K-proton channels first proposed for the *P. denitrificans* and bovine enzymes (7,8). (The amino acid residues defined for each channel are the ones considered to be important for the catalytic and/or pumping mechanisms in A1-type enzymes. Throughout the text, unless otherwise stated, the amino acid numbering of *Paracoccus denitrificans* aa_3 oxygen reductase is used.) In addition to AspI-124 (D) close to the negative side of the membrane, for which the channel is named, the D-channel contains hydrophilic amino acid residues (AsnI-199, AsnI-113, AsnI-131, TyrI-35, SerI-134, and SerI-193) ending at a glutamyl, GluI-278, that is considered by many authors to be a key residue in the operating mechanism of heme-copper enzymes. The residues LysI-354 (K), ThrI-351, SerI-291, and TyrI-280 are part of the K-channel (3,5,7–9). The enzymes belonging to the A2 subfamily (e.g., the caa_3 oxygen reductases from *Rhodothermus marinus* and *Thermus thermophilus*) have all of those amino acid residues, with the exception of the glutamate residue present at the hydrophilic end of the D-channel (4). According to a structural homology model built for *R. marinus* caa_3 (10), the A2-type enzymes have a tyrosine residue whose hydroxyl group was predicted to occupy the spatial place of the carboxyl group of the absent glutamyl. Furthermore, there is a serine residue consecutive to tyrosyl that may also play an important role in proton transfer (11,12). Both A1- and A2-type enzymes completely reduce dioxygen to water and pump protons with similar

Submitted June 16, 2008, and accepted for publication July 18, 2008.

Address reprint requests to Manuela M. Pereira, Instituto de Tecnologia Química e Biológica, Av. da República, EAN, 2780-157 Oeiras, Portugal. Tel.: 351-214469321; Fax: 351-214428314; E-mail: mpereira@itqb.unl.pt.

Editor: Betty J. Gaffney.

0006-3495/08/11/4448/08 $2.00

doi: 10.1529/biophysj.108.139493

stoichiometries, which shows that glutamyl is not essential for the general function of heme-copper oxygen reductases.

To elucidate the molecular mechanism of dioxygen reduction and its coupling to the pumping of protons, the thermodynamic and kinetic characterization of different members of the heme-copper oxygen reductases superfamily is essential. The redox behavior of canonical A1-type enzymes (mitochondrial-like and its close relatives) has been studied through redox titrations monitored by different spectroscopic techniques, such as UV-visible, electron paramagnetic resonance (EPR), magnetic circular dichroism (MCD), infrared (IR) and Fourier transform infrared (FTIR) spectroscopy, and different methods were used to analyze the data. The first experiments performed with intact mitochondria and with the bovine aa_3 oxygen reductase (13–15) led to the proposal that both hemes a and a_3 had distinct reduction potentials. The changes in absorbance of the Soret and α-bands maxima of the electronic spectra of the hemes showed the presence of two transitions with the same amplitude at 380 and 220 mV, which were assigned to the reduction of hemes a_3 and a, respectively. Later, further redox titrations were analyzed considering heme-heme interactions, meaning that their reduction potentials would be dependent on the redox state of the other heme (16–19).

Here we report a study of the thermodynamic redox behavior of two members of the A family (*P. denitrificans* aa_3 and *R. marinus* caa_3 oxygen reductases, belonging to the A1 and A2 subfamilies, respectively) observed at different pH values ranging from 6.0 to 8.0. The results are compared with those previously reported for enzymes belonging to the B and C families (20,21).

MATERIALS AND METHODS

Bacterial growth and protein purification

The caa_3 oxygen reductase from *R. marinus* was purified as described elsewhere (11). *Paracoccus denitrificans* Pd1222 strain was grown aerobically at 30°C in succinate medium, as described by Ludwig (22). Cells were harvested and disrupted in a French press at 9000 psi. Membranes were collected by ultracentrifugation at 138,000 *g* at 4°C during 5 h and solubilized overnight with *n*-dodecyl-β-D-maltoside (DM) in a 1/1 (w/w; detergent/protein) proportion, in 20 mM potassium phosphate pH 7.5 and 1 mM phenylmethanesulfonylfluoride (PMSF), at 4°C. All chromatographic steps were done on a Pharmacia HiLoad system at 4°C. Solubilized membranes were loaded into a Q-Sepharose HP column equilibrated with 20 mM potassium phosphate pH 7.5, 1 mM PMSF and 0.1% DM as buffer, and eluted in a linear gradient of 0–500 mM NaCl in the same buffer. The fraction containing the aa_3 oxygen reductase was applied in a gel filtration S200 column, being eluted with the previous buffer containing 150 mM NaCl. All the purification steps were monitored by visible spectroscopy and SDS-PAGE.

Redox titrations

Fully reversible anaerobic redox titrations were monitored by visible spectroscopy between 380 and 700 nm in a Shimadzu UV-1603 spectrophotometer at 25°C, and at several pH values in a glass cuvette of 1 cm path length and 2.5 mL working volume. Each titration was carried out using 50 mM Mes-Bis-TrisPropane, 0.1% DM as buffer (adjusted to the selected pH value), 1.5 μM purified enzyme, and the following redox mediators at a final concentration of 15 μM: ferrocenecarboxylic acid, potassium ferricyanide, *N*, *N*-dimethyl-*p*-phenylenediamine, *p*-benzoquinone, 1,2-naphthoquinone-4-sulfonic acid, 1,2-naphthoquinone, trimethylhydroquinone, phenazine methosulfate, 1,4-naphthoquinone, duroquinone, and menadione. The redox mediators and their concentrations were chosen so that there would be no spectral interferences and redox equilibration would be maintained. The cuvette was adapted in-house to ensure an anaerobic environment during the titration process. The cuvette and sample were flushed with argon before and during the titration, and the sample was continuously stirred to obtain a homogeneous solution. Sodium dithionite was used as the reductant, and potassium hexachloroiridate (IV) or potassium ferricyanide was used as the oxidant. Reductant and oxidant solutions were prepared in 250 mM Tris-HCl pH 8.7 and 100 mM Tris-HCl pH 7.5, respectively, and made anaerobic by degassing and flushing with argon. These solutions were kept under an argon atmosphere during all the titration. Small additions were made with a 10 μL gas-tight Hamilton syringe to achieve 5–10 mV oxidation/reduction steps. A combined silver/silver chloride electrode was used, calibrated with a saturated quinhydrone solution at pH 7.0 and 25°C. The reduction potentials are quoted versus the standard hydrogen electrode.

Data analysis

The data were analyzed using MATLAB (The MathWorks, Natick, MA) software. For each enzyme and pH value, the spectrum of the fully oxidized enzyme was subtracted from each of the other (partially or fully reduced) spectra measured along the redox titration. Both hemes a and a_3 have their absorption maxima within the same wavelengths region. The maxima at the Soret and α regions of the spectral differences (at 446 and 605 nm for the aa_3 enzyme from *P. denitrificans*, and at 444 and 604 nm for the caa_3 enzyme from *R. marinus*) were then used to describe the redox behavior of hemes a and a_3. For the *R. marinus* enzyme, the redox behavior of the subunit II heme c was monitored at its α-band maximum, 551 nm. By normalizing these absorbance changes, the redox profiles of hemes a, a_3, and c were obtained at each pH value and subsequently their pH dependence was determined.

The data collected for hemes a and a_3 were analyzed assuming a system of two interacting redox centers that describes the thermodynamic behavior involving four different redox microstates as shown in Fig. 1 (20,21). The fully reduced microstate (0,0) was considered the reference state; however, other states (e.g., the fully oxidized state (1,1)) could be chosen. In this case the reference reduction potentials (e_a and e_{a3}) can be defined as the reduction potential of the heme when the other remains in the (reference) reduced state; sometimes these e_a and e_{a3} are called the low asymptotic value of the reduction potential. The fit of the data at the Soret and α-bands for both hemes a and a_3 took into account the difference between their molar absorption coefficients at each wavelength. According to the literature (23,24), heme a and heme a_3 have different molar absorption coefficients in the Soret and

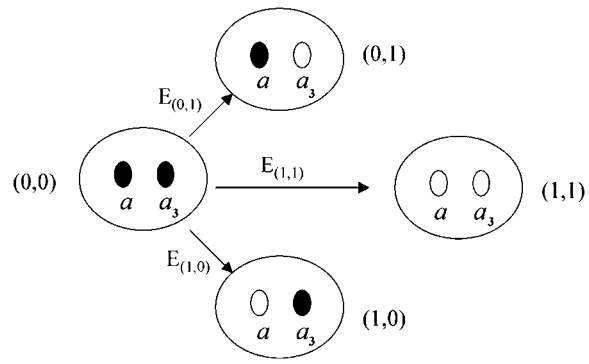

FIGURE 1 Schematic representation of the redox behavior of a system with two interacting redox centers. (O) oxidized center; (●) reduced center.

α-bands, being the first responsible for ~80% and 45% of the total absorbance at the α and Soret bands, respectively. The reference reduction potentials and interaction potentials (e_a, e_{a3}, and I_{aa3}) were obtained from the best fit performed to the experimental results using the nonlinear least-squares Marquardt-Levenberg algorithm (as implemented in the Gnuplot program (25)). Fitting the experimental data recorded at two wavelengths simultaneously, and introducing different molar absorption coefficients for the hemes, allowed the determination of the two reference reduction potentials and the interaction parameter. The relative populations of the four different microstates (Fig. 1) were determined at each solution redox potential. To individualize the redox profile of each heme (a and a_3), the sum of the relative populations of the two microstates in which each heme is reduced (for heme a: ($a_a = 0, a_{a3} = 1$) and ($a_a = 0, a_{a3} = 0$); for heme a_3: ($a_a = 1, a_{a3} = 0$) and ($a_a = 0, a_{a3} = 0$)) was determined. The midpoint reduction potentials were thus unequivocally determined as the solution redox potential at which half of the heme a or a_3 populations were reduced. The equilibrium constant for the electron transfer between hemes a and a_3 was determined by the following equation

$$K_{eq} = P(a_a = 0, a_{a3} = 1)/P(a_a = 1, a_{a3} = 0), \qquad (1)$$

where P represents the probability of the microstate.

The data recorded at 551 nm, describing the redox profile of heme c from the caa_3 oxygen reductase, were analyzed using a single-electron Nernst equation.

RESULTS

Several reversible redox titrations of the aa_3 and caa_3 oxygen reductases were carried out at different pH values to determine the midpoint reduction potential of the hemes, as well as their pH dependence.

Fig. 2 shows the visible spectra taken along the titrations of the aa_3 and caa_3 enzymes at pH 7.5. The redox profile of hemes a and a_3 is dependent on pH, as exemplified at pH 6.0 and 7.5 for the aa_3 enzyme (Fig. 3), and at pH 7.0 and 7.5 for the caa_3 enzyme (Fig. 4). By fitting the data to the appropriate equations for two interacting redox centers (see Materials and Methods section), reference reduction potentials of 283 and 229 mV for hemes a and a_3 and an interaction potential of -20 mV were obtained for the aa_3 enzyme at pH 7.5 (Fig. 3). For the caa_3 enzyme at the same pH, reference reduction potentials of 230 and 182 mV for hemes a and a_3, respectively, and an interaction potential of -54 mV were determined (Fig. 4). The data collected at other pH values were analyzed similarly (Figs. 3 and 4, Tables 1 and 2). The calculated populations of the four possible microstates (Fig. 1) are shown in Fig. 5 for the aa_3 and caa_3 enzymes at pH 7.5. It is clear that when the average number of electrons present in hemes a and a_3 is one (at their joint half reduction), the relative populations of the four microstates are different (Tables 3 and 4). For both enzymes, the probabilities of microstates (0,1), corresponding to heme a reduced and heme a_3 oxidized, are larger than those of microstates (1,0), which corresponds to the inverse situation, indicating that the midpoint reduction potential of heme a is higher than that of a_3. From the relative populations of these microstates, the equilibrium constant that describes the electron transfer between microstates (0,1) and (1,0) can be calculated for all the pH values. Equilibrium constants of 8.2 for the *P. denitrificans* enzyme and 6.5 for the *R. marinus* enzyme at pH 7.5 were determined, indicating that the equilibrium is shifted toward the reduction of the low-spin heme a (Tables 3 and 4).

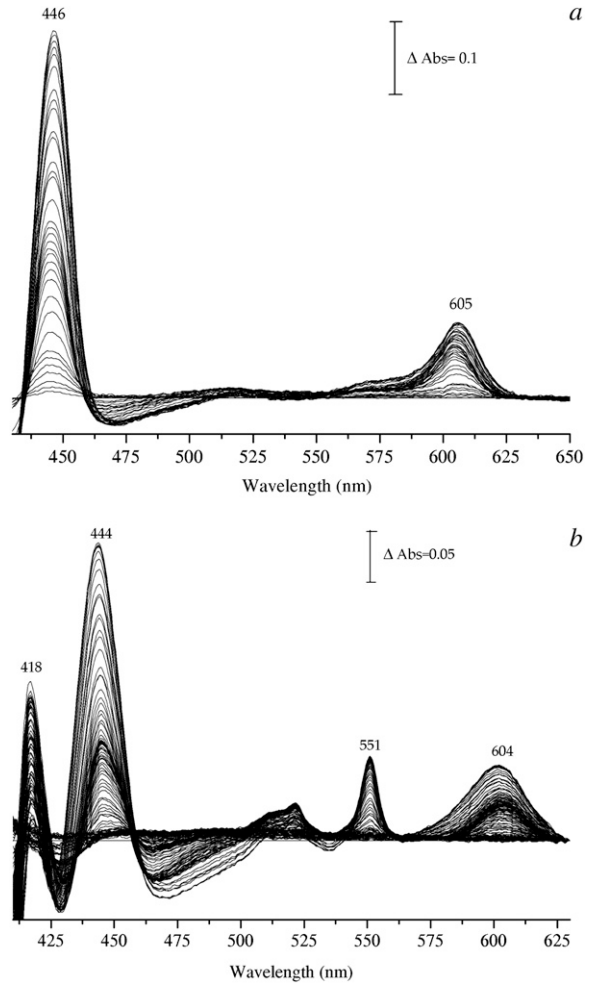

FIGURE 2 Difference of the spectra of the successive partially reduced oxygen reductases minus that of their fully oxidized form at pH 7.5. (*a*) aa_3 from *P. denitrificans*. (*b*) caa_3 from *R. marinus*. The spectra correspond to the reductive titrations, from 500 to 0 mV.

The midpoint reduction potentials for hemes a and a_3 for both enzymes were determined. This parameter is independent of the chosen reference state and is the solution redox potential at which half of the heme population is in the reduced state, i.e., the redox potential at which the heme redox state shows a higher variability (this information is not provided by the reference reduction potentials). The midpoint reduction potential of a heme depends on its intrinsic potential (the reduction potential that it would have if there were no other redox centers) and its possible interactions with other redox centers. Both the intrinsic reduction potential and interactions may also be affected by possible protonation/deprotonation equilibria of protonatable sites. At pH 7.5, hemes a and a_3 from the *P. denitrificans* aa_3 oxygen reductase have midpoint reduction potentials of 301 and 231 mV, whereas those of the *R. marinus* enzyme are 280 and 186 mV. Table 5 shows the values obtained at all pH values.

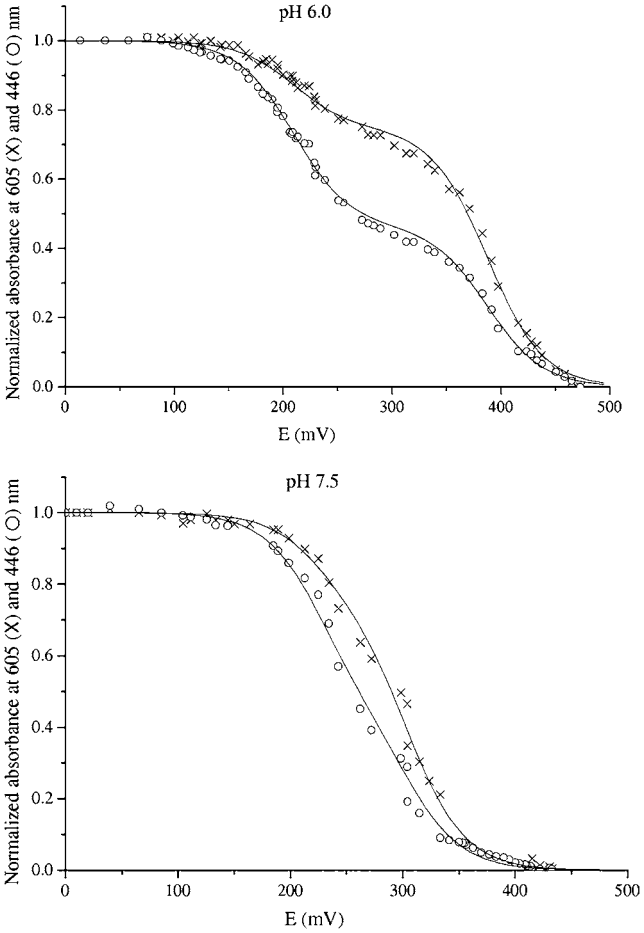

FIGURE 3 Reductive titration curves obtained for *P. denitrificans* aa_3 oxygen reductase at pH 6.0 (*upper panel*) and pH 7.5 (*lower panel*). Data collected at the Soret and α-band maxima, 446 nm (O), and 605 nm (×), respectively. Solid lines are the best fits obtained by the pairwise model for two interacting centers (see Materials and Methods section). The reference reduction potentials and interaction potentials are presented in Table 3.

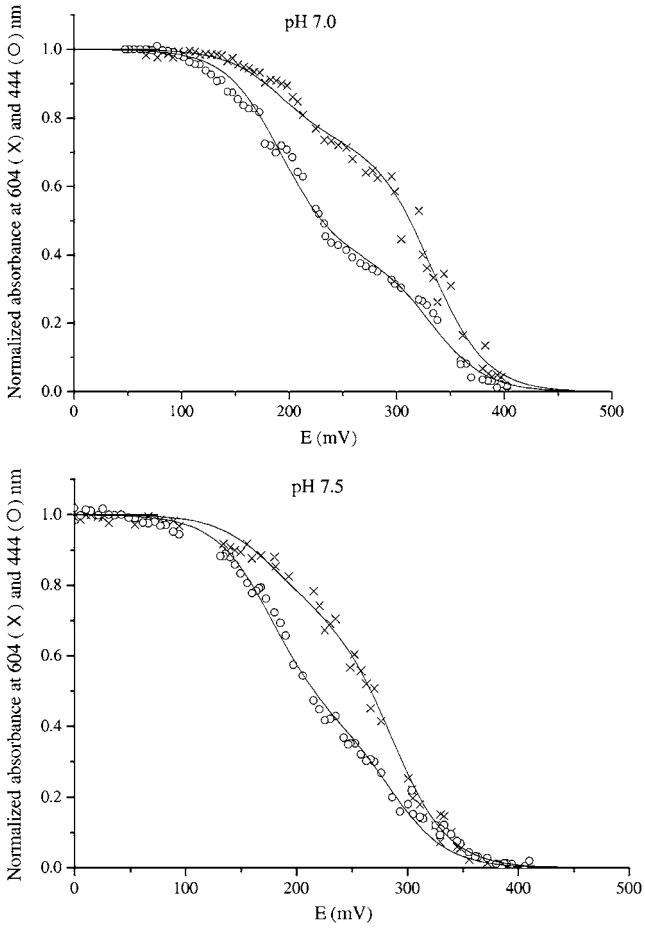

FIGURE 4 Reductive titration curves obtained for *R. marinus* caa_3 oxygen reductase at pH 7.0 (*upper panel*) and pH 7.5 (*lower panel*). Data collected at the Soret and α-band maxima, 444 nm (O), and 604 nm (×), respectively. Solid lines are the best fits obtained by the pairwise model for two interacting centers (see Materials and Methods section). The reference reduction potentials and interaction potentials are presented in Table 4.

The redox behavior of heme *c* from the caa_3 oxygen reductase was described by a single-electron Nernst equation for the whole pH range, and at pH 7.5 its midpoint reduction potential is 230 mV (Fig. 6).

The pH dependence of the midpoint reduction potentials of the hemes from the two enzymes is displayed in Fig. 7. The lines depicted are just visual guides for that dependence, since the use of some widespread particular functions is inappropriate for the multicenter systems studied here, as discussed elsewhere (20,21). But it is important to emphasize again that a fit with several pKa values would be meaningless in microscopic terms, since multiple ionizable sites undergo protonation/deprotonation events along the reduction of the enzyme. In the aa_3 oxygen reductase from *P. denitrificans*, the low-spin heme *a* has a pH-dependent midpoint reduction potential, whereas the high-spin heme a_3 always has a midpoint reduction potential of ~230 mV within the studied pH range. In the case of the caa_3 enzyme from *R. marinus*, the opposite is observed: the midpoint reduction potential of the high-spin heme a_3 is pH dependent, but that of the low-spin heme *a* does not show a significant change with pH. The midpoint reduction potential of heme *c* present in subunit II of the caa_3 enzyme is also pH dependent (Fig. 7).

DISCUSSION

The aim of this study of heme-copper oxygen reductases was to thoroughly characterize several properties of representa-

TABLE 1 Reference reduction potentials (e_a and e_{a3}) and interaction potential (I_{aa3}) for hemes *a* and a_3 from *P. denitrificans* aa_3 oxygen reductase

pH	e_a (mV)	e_{a3} (mV)	I_{aa3} (mV)
6.0	274	213	−112
6.5	292	245	−60
7.0	254	218	−75
7.5	283	229	−20
8.0	287	230	−34

TABLE 2 Reference reduction potentials (e_a and e_{a3}) and interaction potential (I_{aa3}) for hemes *a* and a_3 from *R. marinus caa*$_3$ oxygen reductase

pH	e_a (mV)	e_{a3} (mV)	I_{aa3} (mV)
6.0	245	237	−69
6.5	260	229	−56
7.0	251	195	−78
7.5	230	182	−54
7.75	227	170	−92
8.0	214	171	−81

tive members of the different families to investigate which properties or features are common to all members of this widespread superfamily. Those strictly conserved elements should be on the basis of a common mechanism able to describe the general operating mode of all these enzymes. The first parameters chosen for this comprehensive study were the

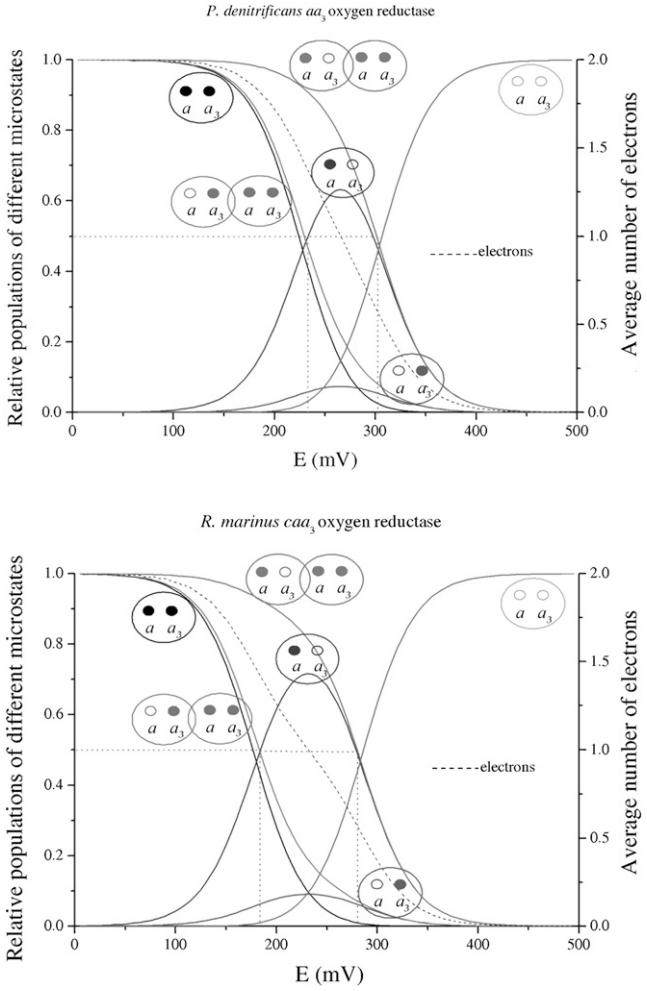

FIGURE 5 Relative populations of the different microstates (*solid lines*) and average number of electrons (*dashed line*) for the aa_3 enzyme from *P. denitrificans* (*upper panel*) and the caa_3 enzyme from *R. marinus* (*lower panel*), at pH 7.5. Microstate probabilities were obtained from the pairwise interacting redox centers model applied to describe the reductive profile of hemes *a* and a_3 in both enzymes.

TABLE 3 Relative populations of the different microstates when the total average number of electrons loaded on hemes *a* and a_3 is one (at their joint half reduction potential, E_{a+a3}), at different pH values, according to the pairwise model for two interacting centers for *P. denitrificans aa*$_3$ oxygen reductase

pH	(1,1) %	(0,1) %	(1,0) %	(0,0) %	*K*eq	(0,0) + (0,1) %	(0,0) + (1,0) %	E_{a+a3} (mV)
6.0	2.9	86.0	8.0	3.1	10.8	89.1	11.1	300
6.5	8.7	70.8	11.4	9.0	6.2	79.9	20.4	299
7.0	7.7	67.7	16.7	7.9	4.1	75.6	24.6	274
7.5	14.8	62.7	7.7	14.8	8.2	77.5	22.5	266
8.0	12.0	69.0	7.5	11.5	9.2	80.5	19.0	275

Microstates are shown as (a_a, a_{a3}), where $a = 0$ or 1 depending on whether the heme is reduced or oxidized, respectively.

redox/thermodynamic properties of the heme centers. By using the same explicit methodology, one can perform a reliable comparison of the different enzymes.

The thermodynamic redox behavior of the A-type hemes of both enzymes was analyzed assuming an interaction of two redox centers, as discussed in the Materials and Methods section. Because of the proximity of the two hemes with a third redox entity, the copper center Cu_B, the presence of electrostatic interactions between these centers may be relevant to the redox behavior of the hemes. It is important to stress that in this case a pairwise function for three interacting redox centers, with three reference reduction potentials and three interaction parameters used as variables, might be more appropriate. However, recent results suggest that the Cu_B center is the first final electron acceptor upon reduction of the fully oxidized aa_3 oxygen reductase with the first electron, i.e., the thermodynamic equilibrium is reached (26). Therefore, when the hemes start to titrate under equilibrium situations, Cu_B is already reduced and its interference will remain constant along the reduction of the hemes. The results presented here for the aa_3 and caa_3 oxygen reductases show that hemes *a* and a_3 have different intrinsic and midpoint reduction potentials. Within the studied pH range, the probability of heme *a* being reduced and heme a_3 oxidized (represented by microstate (0,1)) is always higher than the probability of

TABLE 4 Relative populations of the different microstates when the total average number of electrons loaded on hemes *a* and a_3 is one (at their joint half reduction potential, E_{a+a3}), at different pH values, according to the pairwise model for two interacting centers for *R. marinus caa*$_3$ oxygen reductase

pH	(1,1) %	(0,1) %	(1,0) %	(0,0) %	*K*eq	(0,0) + (0,1) %	(0,0) + (1,0) %	E_{a+a3} (mV)
6.0	10.4	45.9	33.6	10.1	1.4	56.0	43.7	275
6.5	11.2	60.1	17.9	10.8	3.3	70.9	28.7	272
7.0	5.8	79.4	9.0	5.8	8.9	85.2	14.8	262
7.5	9.6	70.0	10.8	9.6	6.5	79.6	20.4	233
7.75	4.6	82.1	8.9	4.4	9.2	86.5	13.3	244
8.0	6.3	73.2	13.7	6.8	5.3	80.0	20.5	234

Microstates are shown as (a_a, a_{a3}), where $a = 0$ or 1 depending on whether the heme is reduced or oxidized, respectively.

TABLE 5 Midpoint reduction potentials for the heme centers of *P. denitrificans* aa_3 and *R. marinus* caa_3 oxygen reductases

	P. denitrificans aa_3 oxygen reductase		*R. marinus* caa_3 oxygen reductase		
pH	E_a (mV)	E_{a3} (mV)	E_a (mV)	E_{a3} (mV)	E_c (mV)
6.0	384	215	290	260	250
6.5	349	249	309	236	235
7.0	322	225	326	198	235
7.5	301	231	280	186	230
7.75	nd	nd	316	173	220
8.0	318	232	290	177	195

nd, not determined.

the inverse situation represented by microstate (1,0); in particular, this holds when both hemes have an average joint occupancy of one electron. From the relative populations of these microstates, the equilibrium constant that describes the electron transfer between microstates (0,1) and (1,0) can be calculated for all the pH values. It was observed that it is always higher than one for both enzymes, indicating that the equilibrium is shifted toward the reduction of the low-spin heme *a*. These results show unequivocally that heme *a* and heme a_3 have different midpoint reduction potentials. It is also shown that the pH dependence of the midpoint reduction potentials of the hemes differs between the two members of the A family.

Several studies of the redox properties of A1-type enzymes, namely the mitochondrial and *P. denitrificans* aa_3 oxygen reductases, have already been reported (16,19,27–32). However, there are only a few reports regarding the redox behavior of enzymes from the A2 subfamily (namely, the caa_3 enzyme from *T. thermophilus* (33,34)) and some preliminary studies on the *R. marinus* caa_3 enzyme (11).

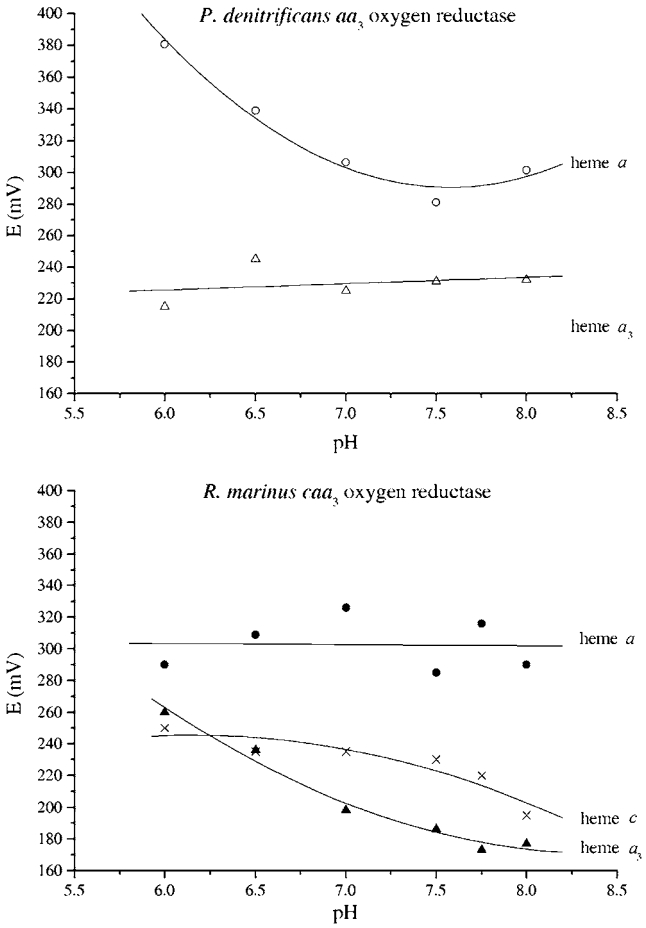

FIGURE 7 pH dependence of the midpoint reduction potentials of the heme centers of the aa_3 oxygen reductase from *P. denitrificans* (upper panel) and the caa_3 oxygen reductase from *R. marinus* (lower panel). *P. denitrificans* aa_3 oxygen reductase: hemes *a* (O) and a_3 (△). *R. marinus* caa_3 oxygen reductase: hemes *a* (●), a_3 (▲), and heme *c* (×). Solid lines were adjusted to the experimental data for better visualization of the pH dependence of the midpoint reduction potentials of the hemes.

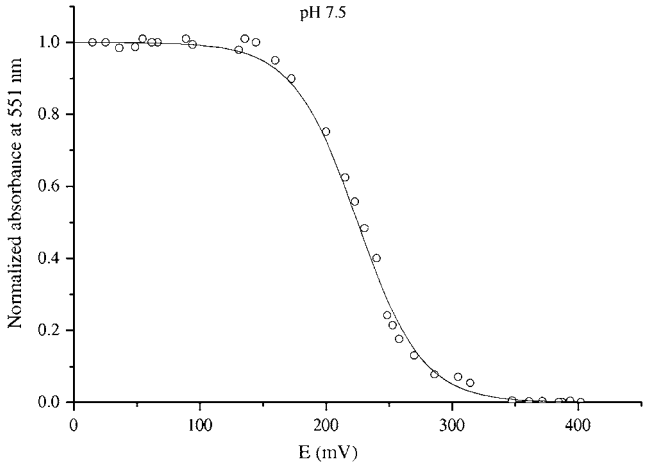

FIGURE 6 Heme *c* reduction titration curve obtained for *R. marinus* caa_3 oxygen reductase at pH 7.5. Data collected at the α-band maximum 551 nm (Δ). The solid line was obtained by fitting a single-electron Nernst curve with $E = 230$ mV.

The results presented here for the aa_3 oxygen reductase from *P. denitrificans* contrast with those recently obtained by potentiometric redox titrations monitored by FTIR spectroscopy (16). It was proposed that hemes *a* and a_3 have similar midpoint reduction potentials within the studied pH range, meaning that each electron loaded would be equally shared by the two hemes. The presence of redox interactions between these heme centers was also proposed, as well as a pH dependence of ~30 mV/pH unit for the reduction potentials of the hemes and for the interaction potential between them. It has also been proposed for the same enzyme that hemes *a* and a_3 had distinct reduction potentials based on results obtained by oxidative redox titrations at pH 6.9, monitored by visible spectroscopy (35). However, in that case, the redox behavior of the hemes was analyzed at a single wavelength and described by the sum of two independent single-electron Nernst equations with distinct re-

duction potentials, without taking into account the presence of redox interactions. The redox properties of the hemes of two members of the A2 subfamily have already been reported (11,33,34) and in those cases the reductive profile of hemes *a* and a_3 was also monitored only at a single wavelength, and the reduction potentials were determined by independent Nernst equations with different relative contributions. In both cases, the presence of redox interactions between the hemes was not considered. A direct comparison between the results reported here and those previously presented by other authors is hampered due to differences in the methodologies used to analyze the data.

For the A2-type caa_3 oxygen reductase studied here, the reductive profile of the heme *c* located at subunit II was analyzed independently of the A-type hemes from the catalytic subunit. Even without three-dimensional structural data regarding the localization of the heme *c* domain with respect to the A-type hemes, they were considered to be positioned at a distance >20 Å, at which Cu_A is located in A- and B-type enzymes (7,36). At such a distance, heme *c* would probably not interact with the other hemes, although possible electrostatic interactions between heme *c* and the Cu_A center cannot be excluded. In this study, since the data do not show any deviation from single-electron Nernst behavior, it appears that such redox interactions are negligible. Previous studies performed with the truncated version of the *R. marinus* caa_3 cytochrome *c* domain showed that the midpoint reduction potential of heme *c* was pH independent between pH 6.5 and 8.0 (37), which contrasts with the results obtained here. This discrepancy most probably results from the different environments that surround heme *c* when it is inserted into a large complex, or in its truncated, isolated version.

We recently presented redox/thermodynamic data for members of the B and C families (20,21). For the chosen B-type enzyme, the ba_3 oxygen reductase from *T. thermophilus*, it was observed that the relative order of the midpoint reduction potentials of the low- and high-spin hemes changes significantly with pH. At pH 7.0, the high-spin heme a_3 has a higher midpoint reduction potential than the low-spin heme *b*, but at pH 8.4 the opposite is observed (20). This relation of the midpoint reduction potentials had been already observed for this enzyme in a single redox titration at pH 7.0 (38) and for the aa_3 oxygen reductase from *Acidianus ambivalens*, also a member of the B family, using resonance Raman spectroscopy (39). These data corroborate the proposal that in these enzymes the high-spin heme has a higher midpoint reduction potential than that of the low-spin heme at pH lower than 8.0. For the cbb_3 oxygen reductase from *Bradyrhizobium japonicum*, a C-type enzyme, we observed that the low-spin heme *b* has a higher midpoint reduction potential than the high-spin heme b_3 within the studied pH range, and that the midpoint reduction potentials of both hemes were pH dependent. In addition to hemes *b* and b_3 present in the catalytic subunit, these enzymes also have dihemic and monohemic cytochrome *c* subunits. The redox behavior of these three C-type hemes was also studied, and it was shown that their midpoint reduction potentials were pH dependent (21).

In redox-driven proton pumps, such as heme-copper oxygen reductases, studies of the redox behavior of each redox center and its pH dependence are crucial for elucidating the catalytic and pumping mechanisms, as well as the coupling of these two processes.

CONCLUSIONS

In conclusion, despite the fact that only one representative member of each family was extensively studied, the results indicate significant differences between the families of heme-copper oxygen reductases: neither the relative order of the midpoint reduction potentials of the hemes nor their pH dependence is common among the different families. The hypothesis that each family of enzymes has different mechanisms to perform the same function cannot be excluded, but the structural similarities between these enzymes seem to favor the existence of similar catalytic, pumping, and e/H^+ coupling mechanisms. The pH dependence of the midpoint reduction potential of the hemes reported here shows the existence of a thermodynamic linkage between electron and proton transfer steps, which is important for proton uptake and/or translocation. Within the framework of a common mechanism in heme-copper enzymes, the different relative orders and pH dependences of the midpoint reduction potentials of the hemes affect in different ways the electron transfer kinetics, the relative order of intramolecular electron distribution, and the precise events of electron-proton coupling, but the basic principles that govern these mechanisms should be similar.

Andreia F. Veríssimo and Filipa L. Sousa are recipients of grants from Fundação para a Ciência e a Tecnologia (SFRH XXI/BD/14388/2003 and SFRH XXI/BD/27972/2006, respectively). This work was supported by Fundação para a Ciência e a Tecnologia (POCTI/QUI/66559/2006 to M.P. and POCI/BIA-PRO/58608/2004 to M.T.). Professor Bernd Ludwig is acknowledged for providing the *P. denitrificans* Pd1222 strain. João Carita (ITQB) is acknowledged for cell growth.

REFERENCES

1. Garcia-Horsman, J. A., B. Barquera, J. Rumbley, J. Ma, and R. B. Gennis. 1994. The superfamily of heme-copper respiratory oxidases. *J. Bacteriol.* 176:5587–5600.
2. Ferguson-Miller, S., and G. T. Babcock. 1996. Heme/copper terminal oxidases. *Chem. Rev.* 96:2889–2908.
3. Hosler, J. P., S. Ferguson-Miller, and D. A. Mills. 2006. Energy transduction: proton transfer through the respiratory complexes. *Annu. Rev. Biochem.* 75:165–187.
4. Pereira, M. M., M. Santana, and M. Teixeira. 2001. A novel scenario for the evolution of haem-copper oxygen reductases. *Biochim. Biophys. Acta.* 1505:185–208.
5. Michel, H., J. Behr, A. Harrenga, and A. Kannt. 1998. Cytochrome *c* oxidase: structure and spectroscopy. *Annu. Rev. Biophys. Biomol. Struct.* 27:329–356.
6. Pereira, M. M., and M. Teixeira. 2004. Proton pathways, ligand binding and dynamics of the catalytic site in haem-copper oxygen reductases:

a comparison between the three families. *Biochim. Biophys. Acta.* 1655:340–346.

7. Iwata, S., C. Ostermeier, B. Ludwig, and H. Michel. 1995. Structure at 2.8 A resolution of cytochrome *c* oxidase from *Paracoccus denitrificans*. *Nature*. 376:660–669.
8. Tsukihara, T., H. Aoyama, E. Yamashita, T. Tomizaki, H. Yamaguchi, K. Shinzawa-Itoh, R. Nakashima, R. Yaono, and S. Yoshikawa. 1995. Structures of metal sites of oxidized bovine heart cytochrome *c* oxidase at 2.8 A. *Science*. 269:1069–1074.
9. Gennis, R. B. 1998. Multiple proton-conducting pathways in cytochrome oxidase and a proposed role for the active-site tyrosine. *Biochim. Biophys. Acta*. 1365:241–248.
10. Soares, C. M., A. M. Baptista, M. M. Pereira, and M. Teixeira. 2004. Investigation of protonatable residues in *Rhodothermus marinus caa3* haem-copper oxygen reductase: comparison with *Paracoccus denitrificans aa3* haem-copper oxygen reductase. *J. Biol. Inorg. Chem.* 9: 124–134.
11. Pereira, M. M., M. Santana, C. M. Soares, J. Mendes, J. N. Carita, A. S. Fernandes, M. Saraste, M. A. Carrondo, and M. Teixeira. 1999. The *caa3* terminal oxidase of the thermohalophilic bacterium *Rhodothermus marinus*: a HiPIP:oxygen oxidoreductase lacking the key glutamate of the D-channel. *Biochim. Biophys. Acta*. 1413:1–13.
12. Santana, M., M. M. Pereira, N. P. Elias, C. M. Soares, and M. Teixeira. 2001. Gene cluster of *Rhodothermus marinus* high-potential iron-sulfur protein: oxygen oxidoreductase, a *caa*(3)-type oxidase belonging to the superfamily of heme-copper oxidases. *J. Bacteriol.* 183:687–699.
13. Tiesjema, R. H., A. O. Muijsers, and B. F. van Gelder. 1973. Biochemical and biophysical studies on cytochrome *c* oxidase. X. Spectral and potentiometric properties of the hemes and coppers. *Biochim. Biophys. Acta*. 305:19–28.
14. Wilson, D. F., J. G. Lindsay, and E. S. Brocklehurst. 1972. Heme-heme interaction in cytochrome oxidase. *Biochim. Biophys. Acta*. 256:277–286.
15. Wilson, D. F., and J. S. Leigh, Jr. 1972. Heme-heme interaction in cytochrome *c* oxidase in situ as measured by EPR spectroscopy. *Arch. Biochem. Biophys.* 150:154–163.
16. Gorbikova, E. A., K. Vuorilehto, M. Wikstrom, and M. I. Verkhovsky. 2006. Redox titration of all electron carriers of cytochrome *c* oxidase by Fourier transform infrared spectroscopy. *Biochemistry*. 45:5641–5649.
17. Malmström, B. G. 1974. Cytochrome *c* oxidase: some current biochemical and biophysical problems. *Q. Rev. Biophys.* 6:389–431.
18. Wikstrom, K. F., H. J. Harmon, W. J. Ingledew, and B. Chance. 1976. A re-evaluation of the spectral, potentiometric and energy-linked properties of cytochrome *c* oxidase in mitochondria. *FEBS Lett*. 65: 259–277.
19. Wikstrom, M., K. Krab, and M. Saraste. 1981. Cytochrome Oxidase, a Synthesis. Academic Press, New York.
20. Sousa, F. L., A. F. Verissimo, A. M. Baptista, T. Soulimane, M. Teixeira, and M. Pereira. 2008. Redox properties of *Thermus thermophilus ba3*: different electron-proton coupling in oxygen reductases? *Biophys. J.* 94:2434–2441.
21. Verissimo, A. F., F. L. Sousa, A. M. Baptista, M. Teixeira, and M. M. Pereira. 2007. Thermodynamic redox behavior of the heme centers of *cbb3* heme-copper oxygen reductase from *Bradyrhizobium japonicum*. *Biochemistry*. 46:13245–13253.
22. Ludwig, B. 1986. Cytochrome *c* oxidase from *Paracoccus denitrificans*. *Methods Enzymol.* 126:153–159.
23. Liao, G. L., and G. Palmer. 1996. The reduced minus oxidized difference spectra of cytochromes *a* and *a*3. *Biochim. Biophys. Acta*. 1274:109–111.
24. Vanneste, W. H. 1966. The stoichiometry and absorption spectra of components *a* and *a*-3 in cytochrome *c* oxidase. *Biochemistry*. 5:838–848.
25 Williams T., C. Kelley. 1993. Gnuplot, an interactive plotting program. Version 4.0: Copyright 2004–2007. Available at http://www.gnuplot.info/docs/gnuplot.html.
26. Belevich, I., D. A. Bloch, N. Belevich, M. Wikstrom, and M. I. Verkhovsky. 2007. Exploring the proton pump mechanism of cytochrome *c* oxidase in real time. *Proc. Natl. Acad. Sci. USA*. 104:2685–2690.
27. Hendler, R. W., K. V. Reddy, R. I. Shrager, and W. S. Caughey. 1986. Analysis of the spectra and redox properties of pure cytochromes *aa3*. *Biophys. J.* 49:717–729.
28. Pardhasaradhi, K., B. Ludwig, and R. W. Hendler. 1991. Potentiometric and spectral studies with the two-subunit cytochrome *aa3* from *Paracoccus denitrificans*. Comparison with the 13-subunit beef heart enzyme. *Biophys. J.* 60:408–414.
29. Hellwig, P., C. Ostermeier, H. Michel, B. Ludwig, and W. Mantele. 1998. Electrochemically induced FT-IR difference spectra of the two- and four-subunit cytochrome *c* oxidase from *P. denitrificans* reveal identical conformational changes upon redox transitions. *Biochim. Biophys. Acta*. 1409:107–112.
30. Harmon, P. A., R. W. Hendler, and I. W. Levin. 1994. Resonance Raman and optical spectroscopic monitoring of heme *a* redox states in cytochrome *c* oxidase during potentiometric titrations. *Biochemistry*. 33:699–707.
31. Blair, D. F., W. R. Ellis, Jr., H. Wang, H. B. Gray, and S. I. Chan. 1986. Spectroelectrochemical study of cytochrome *c* oxidase: pH and temperature dependences of the cytochrome potentials. Characterization of site-site interactions. *J. Biol. Chem.* 261:11524–11537.
32. Kojima, N., and G. Palmer. 1983. Further characterization of the potentiometric behavior of cytochrome oxidase. Cytochrome α stays low spin during oxidation and reduction. *J. Biol. Chem.* 258:14908–14913.
33. Hellwig, P., T. Soulimane, and W. Mantele. 2002. Electrochemical, FT-IR and UV/VIS spectroscopic properties of the *caa3* oxidase from *T. thermophilus*. *Eur. J. Biochem.* 269:4830–4838.
34. Yoshida, T., and J. A. Fee. 1985. Potentiometric study of cytochrome *c1aa3* from *Thermus thermophilus*. *J. Inorg. Biochem.* 23:279–288.
35. Hellwig, P., S. Grzybek, J. Behr, B. Ludwig, H. Michel, and W. Mantele. 1999. Electrochemical and ultraviolet/visible/infrared spectroscopic analysis of heme *a* and *a3* redox reactions in the cytochrome *c* oxidase from *Paracoccus denitrificans*: separation of heme *a* and *a3* contributions and assignment of vibrational modes. *Biochemistry*. 38:1685–1694.
36. Soulimane, T., G. Buse, G. P. Bourenkov, H. D. Bartunik, R. Huber, and M. E. Than. 2000. Structure and mechanism of the aberrant *ba*(3)-cytochrome *c* oxidase from *Thermus thermophilus*. *EMBO J.* 19:1766–1776.
37. Srinivasan, V., C. Rajendran, F. L. Sousa, A. M. Melo, L. M. Saraiva, M. M. Pereira, M. Santana, M. Teixeira, and H. Michel. 2005. Structure at 1.3 A resolution of *Rhodothermus marinus caa*(3) cytochrome *c* domain. *J. Mol. Biol.* 345:1047–1057.
38. Hellwig, P., T. Soulimane, G. Buse, and W. Mantele. 1999. Electrochemical, FTIR, and UV/VIS spectroscopic properties of the *ba*(3) oxidase from *Thermus thermophilus*. *Biochemistry*. 38:9648–9658.
39. Todorovic, S., M. M. Pereira, T. M. Bandeiras, M. Teixeira, P. Hildebrandt, and D. H. Murgida. 2005. Midpoint potentials of hemes *a* and *a*3 in the quinol oxidase from *Acidianus ambivalens* are inverted. *J. Am. Chem. Soc.* 127:13561–13566.